Establishing Rod-Shape from Spherical, Peptidoglycan-Deficient Bacterial Spores

Huan Zhang[1], Garrett A. Mulholland[1], Sofiene Seef[2], Shiwei Zhu[3,4], Jun Liu[3,4], Tâm Mignot[2] and Beiyan Nan[1]*

[1]Department of Biology, Texas A&M University, College Station, TX 77843, USA
[2]Laboratoire de Chimie Bactérienne, CNRS - Université Aix Marseille UMR7283, Institut de Microbiologie de la Méditerranée, 13009 Marseille, France
[3]Department of Microbial Pathogenesis, Yale University School of Medicine, New Haven, CT 06536, USA
[4]Microbial Sciences Institute, Yale University, West Haven, CT 06516, USA

*Corresponding author: Beiyan Nan, 306C BSBE, 3258 TAMU, College Station, TX77843, Tel.: 979-845-3487, email: bnan@tamu.edu

Keywords: germination, Rod system, MreB, GTPase, gliding motility

ABSTRACT

Chemical-induced spores of the Gram-negative bacterium *Myxococcus xanthus* are peptidoglycan (PG)-deficient. It is unclear how these spherical spores germinate into rod-shaped, walled cells without preexisting PG templates. We found that germinating spores first synthesize PG randomly on spherical surfaces. MglB, a GTPase activating protein, surveys the status of PG growth and establishes one future cell pole. Following MglB, the Ras family GTPase MglA localizes to the second pole. MglA directs molecular motors to transport the bacterial actin homolog MreB and the Rod PG synthesis complexes away from poles. The Rod system establishes rod-shape by elongating PG at nonpolar regions. Thus, the interaction between GTPase, cytoskeletons and molecular motors provides a mechanism for the *de novo* establishment of rod-shape in bacteria.

30 **Significance**

31 Spheres and rods are among the most common shapes adopted by walled bacteria, in which
32 the peptidoglycan (PG) cell wall largely determines cell shape. When induced by chemicals,
33 rod-shaped vegetative cells of the Gram-negative bacterium *Myxococcus xanthus* thoroughly
34 degrades their PG and shrinks into spherical spores. As these spores germinate, cells rebuild
35 rod-shaped PG without preexisting templates, which provides a rare opportunity to visualize *de*
36 *novo* PG synthesis and bacterial morphogenesis. In this study, we investigated how spherical
37 spores elongation into rods during germination and elucidated a system for rod-shape
38 morphogenesis that includes the Rod PG synthesis system, a GTPase-GAP pair, the MreB
39 cytoskeleton and a molecular motor.

40 Morphogenesis is a fundamental problem in biological systems. Compared to symmetric
41 spheres, rods are asymmetric and polarized. For most rod-shaped bacteria, the
42 peptidoglycan (PG) cell wall defines cell geometry, which is synthesized by two major
43 enzymatic systems. The Rod system consists of RodA, a SEDS-family PG polymerase,
44 PBP2, a member of the class B penicillin-binding proteins (bPBPs), and MreB, a
45 bacterial actin homolog (1-3). MreB orchestrates PG growth by the Rod complexes in
46 response to local cell curvature (4-9). In contrast, class A PBPs (aPBPs) contribute to
47 PG growth independent of MreB (10, 11).
48 *Myxococcus xanthus*, a rod-shaped Gram-negative bacterium, utilizes polarized
49 geometry for directed locomotion. MglA, a Ras family small GTPase, controls the
50 direction of gliding motility. The motors for gliding assemble into functional machineries
51 on MreB filaments (12-16). Consequently, the gliding machineries carry MreB filaments
52 as they move rapidly in the membrane (17). As cells move, GTP-bound MglA forms
53 large clusters at leading cell poles, whereas GDP-bound MglA distributes
54 homogeneously in the cytoplasm (16, 18, 19). The activity of MglA is regulated by its
55 cognate GTPase-activating protein (GAP), MglB, which forms large clusters at lagging
56 cell poles. MglB activates the GTPase activity of MglA, expelling MglA-GTP from
57 lagging poles (18, 19). MglA regulates the assembly and moving direction of the gliding
58 machinery through direct interaction with MreB (16, 20). Overall, the polarized
59 localization and activities of MglA and MglB ensure that the majority of gliding
60 machineries moves from poles to nonpolar regions, which generates propulsion (12, 16,
61 20).

62 Some rod-shaped bacteria change their geometry through sporulation. In
63 Firmicutes such as Bacilli and Clostridia, the morphological differentiation from rod-
64 shaped vegetative cells to oval spores begins with an asymmetric division, resulting in
65 the formation of a smaller spore wholly contained within a larger mother cell. In contrast
66 to endospore-forming bacteria, *M. xanthus* produces spores using two division-
67 independent mechanisms. First, groups of vegetative cells can aggregate on solid
68 surfaces and build spore-filled fruiting bodies (21). Second, individual *M. xanthus* cells
69 can form dispersed, spherical spores in response to chemical signals, such as glycerol
70 (22). Unlike endospores that contain intact and often thickened PG (23, 24), PG is
71 thoroughly degraded during single cell sporulation (25). Without the polarity defined by
72 PG, the mechanism by which glycerol-induced *M. xanthus* spores elongate into rods
73 remains largely unknown.

Results

Two-phase morphological transition during *M. xanthus* spore germination.

Overnight induction by 1 M glycerol produced spores with length to width aspect ratios (L/W) of 1.56 ± 0.36 (n = 789), among which 40.9% are approximately spherical (L/W ≤ 1.3). Overall, the L/W values of most (85.4%) spores were lower than 2. As spores germinated, the morphological transition progressed in a two-phase manner. In the first hour of germination (Phase I), L/W did not change significantly (p = 0.57, Fig. 1A, 1B, *SI Appendix*, Movie S1). After 1 h, L/W increased sharply as the emerging cells transformed into rods (Phase II). 70.2% (n = 198) of emerging cells reached the dimensions of vegetative cells by 3 h (Fig. 1A, 1B, *SI Appendix,* Movie S1, Table S1). After 8 h, the emerging cells are indistinguishable from vegetative cells (L/W = 5.55 ± 1.12, n = 233. Fig. 1A, 1B). Importantly, many oval spores initiated elongation along their short axes (Fig. 1C, *SI Appendix,* Movie S2), indicating that although not perfectly spherical, the geometry of mature spores does not predetermine the polarity of emerging cells.

Using cryo-electron tomography (cryo-ET), we confirmed that mature glycerol-induced spores do not retain PG (*SI Appendix,* Fig. S1). To investigate the role of PG growth in germination, we treated spores with several inhibitors for PG synthesis. In the presence of mecillinam and A22, which inhibit PBP2 and MreB in the Rod system, respectively, spores failed to germinate into rods as their L/W ratios did not increase within 8 h (Fig. 1A, 1B). These treated spores were viable because they were able to grow into rods in inhibitor-free medium. Since A22 and mecillinam-treated spores became even more spherical in Phase I (Fig. 1D), neither inhibitor blocked the

97 hydrolysis of spore coats that maintain the oval shape of spores. In the presence of
98 cefsulodin that inhibits PBP1A/B, and cefmetazole that inhibits all PBPs except PBP2,
99 spores were able to form rods, albeit the elongation rate was slower (Fig. 1A, 1B).
100 Although not essential for rod-like morphogenesis, aPBPs still contribute to the
101 establishment and maintenance of rod shape. First, L/W values of the cefmetazole-
102 treated spores increased significantly in Phase I of germination ($p < 0.0001$, Fig. 1B,
103 1D), suggesting that cells elongate earlier when PBP2 is dominant over other PBPs.
104 Second, despite successful elongation in early Phase II (1 – 3 h), 57.2% (n = 215)
105 cefsulodin-treated and 96.6% (n = 203) cefmetazole-treated emerging cells
106 retrogressed to spheres after 8-h treatments (Fig. 1A, 1B). As glycerol-induced spores
107 preserve PG precursors(25), when fosfomycin was added to inhibit the production of
108 UDP-MurNAc, a precursor of PG, spores were able to elongate into rods (Fig. 1A, 1B).
109 Taken together, PG polymerization by the Rod system is essential for the establishment
110 of rod-shape.
111 We next visualized the patterns of PG growth using a fluorescent D-amino acid,
112 TAMRA 3-amino-D-alanine (TADA) (26) to label newly synthesized PG. To enhance
113 labeling efficiency, we deleted the *dacB* gene (*mxan_3130*), which encodes a D-Ala-D-
114 Ala carboxypeptidase (27). The resulted *ΔdacB* cells showed identical morphology to
115 the wild-type ones and produced sonication-resistant spores. The *ΔdacB* spores
116 showed minor delay in germination and efficient TADA incorporation (Fig. 1E, *SI*
117 *Appendix,* Fig. S2 and Table S1). Although L/W of spores did not change, PG had
118 started to grow in Phase I. The surfaces of most Phase I spores (78.0%, n = 600) were
119 evenly labeled (Fig. 1E). The remaining 22.0% of spores showed bright patches of

120 TADA on their surfaces (Fig. 1F). However, these TADA patches do not likely register
121 future poles because 47.0% (n = 132) of spores contained more than two such patches
122 and these patches positioned randomly on spore surfaces (Fig. 1G, 1F). In contrast, as
123 cells grew into rods, TADA was incorporated heavily at nonpolar regions and
124 fluorescence signals were generally absent at cell poles (Fig. 1E). The patterns of PG
125 growth indicate that spores first synthesize PG on their spherical surfaces in Phase I
126 and then break symmetry in Phase II by growing PG at nonpolar regions.
127 Neither mecillinam, cefsulodin or cefmetazole was able to block TADA
128 incorporation in Phase I of germination. However, a treatment by all three antibiotics
129 abolished TADA incorporation (Fig. 1H), indicating that both aPBPs and the Rod system
130 contribute to the isotropic PG growth in Phase I. In contrast, mecillinam, but not
131 cefsulodin or cefmetazole, blocked TADA incorporation in Phase II of germination (Fig.
132 1H). Consistent with a recent report that cells reduce their diameter when the Rod
133 system becomes dominant over aPBPs (28), emerging cells continued to grow in length
134 but shrink in width in Phase II (Fig. S3). These results confirm that while both aPBPs
135 and the Rod system participate PG synthesis in Phase I of germination, the Rod system
136 plays major roles in cell elongation in Phase II.
137 **MglA and MglB are required for rapid cell elongation** To investigate how *M. xanthus*
138 spores establish cell polarity *de novo*, we tested the potential roles of polar-localized
139 motility regulators. *ΔmglA* and *ΔmglB* cells were able to form sonication-resistant spores
140 but their spores showed severe delays in elongation during germination. After 3 h, only
141 15.7% of the *ΔmglA* (n= 140) and 10.4% of *ΔmglB* (n = 298) cells reached the
142 vegetative aspect ratio (Fig. 2A, 2B). In contrast, deleting *romR* and *plpA*, the genes

143 encode another two polar-localized motility regulators (29-31), only caused minor delay
144 in germination (Fig. S4 and Table S1). Both the *ΔmglA* and *ΔmglB* spores were able to
145 elongate in length and shrink in width, albeit at significantly lower rates (Fig. 2A, 2B, *SI*
146 *Appendix,* Fig. S3), indicating that PG growth by the Rod complex still occurred.
147 Strikingly different from wild-type spores that maintained relatively smooth surfaces
148 during germination, the *ΔmglA* and *ΔmglB* spores generated pronounced bulges at
149 nonpolar regions in Phase II, appearing to have multiple cell poles (Fig. 2A, 2C, *SI*
150 *Appendix,* Movie S3). However, this crooked morphology was largely corrected after
151 prolonged growth (8 h) (Fig. 2A), implying that a system independent of MglA and MglB
152 was able to generate rod shape, although much less robustly. To determine how MglA
153 and MglB regulate germination, we investigated the spores that expressed the $MglA^{Q82L}$
154 variant as the sole source of MglA, under the control of the native promoter of the
155 *mglBA* operon. $MglA^{Q82L}$ expresses normally but is unable to hydrolyze GTP (19).
156 Spores expressing wild-type MglB and $MglA^{Q82L}$ showed both a severe delay in cell
157 elongation and bulged surfaces on emerging cells, similar to the *ΔmglA* and *ΔmglB*
158 spores (Fig. 2A, 2B). Thus, the GTPase activity of MglA is required for rapid cell
159 elongation and MglB functions through MglA.
160 Both the delayed morphological transition and bulged surfaces of the mutant
161 spores suggest that MglA and MglB might regulate PG growth during germination.
162 *ΔmglA ΔdacB* and *ΔmglB ΔdacB* spores were able to grow PG in an isotropic manner in
163 Phase I, identical to the *ΔdacB* spores (Fig. 2D). However, emerging cells from both
164 mutant spores displayed elevated PG growth at cell poles and bulges in Phase II (Fig.
165 2D). As the Rod complex is the major system for PG growth in Phase II, the MglA-MglB

166 polarity axis might promote rapid cell elongation by restricting the Rod complexes to
167 nonpolar regions.

168 **MglB determines the first future pole**. We expressed endogenous YFP-labeled MglA
169 and mCherry-labeled MglB and correlated their localization patterns with L/W. 94.1% (n
170 = 152) of Phase I spores (L/W $\leq$ 2) contained one or two MglB clusters (Fig. 3A, 3B). In
171 phase II spores (L/W > 2), this ratio increased to 100% (n = 120). In contrast, MglA did
172 not form clusters until Phase II, when 54.2% of emerging cells contained one or two
173 MglA clusters (Fig. 3A, 3B). Thus, during germination, MglB establishes polarized
174 localization before MglA.

175 To test if the clusters of MglB in Phase I spores mark the polarity inherited from
176 previous vegetative cells, we imaged MglB clusters at 0.05 Hz. the majority of MglB
177 clusters in Phase I spores was highly dynamic (Fig. 3C, *SI Appendix,* Movie S4). Among
178 114 MglB clusters in Phase I spores, 22.9% remained stationary, and 77.1% showed
179 typical diffusion, with diffusion coefficients (D) of $1.05 \times 10^{-4} \pm 4.62 \times 10^{-5}$ $\mu m^2/s$. These
180 "wandering" MglB clusters were observed in both the approximately spherical (L/W <
181 1.3) and oval spores (1.3 < L/W $\leq$ 2), which supports our hypothesis that, regardless of
182 their geometry, polarity is not yet established in Phase I spores. As a control, imaged at
183 the same frequency, the fluorescence patches of TADA remained stationary in all
184 spores, which excludes potential artifacts caused by the movements of spores (Fig. 3C,
185 *SI Appendix,* Movie S5).

186 As germination progressed to Phase II (L/W > 2), the population of diffusive MglB
187 clusters decreased from 77.1% to 23.6% (n = 106, Fig. 3D). Stabilized MglB clusters
188 oscillated between newly established poles (Fig. 3C, *SI Appendix,* Movie S6), which

189 might provide a mechanism to ensure that MglB occupies each future cell pole for an
190 equal amount of time. When we expressed MglA-YFP in the *ΔmglB* background, the
191 formation of MglA clusters was delayed significantly, and in Phase II of germination,
192 only 23.3% (n = 120) of emerging cells contained MglA clusters (Fig. 3A, 3B). Thus,
193 rods start to form when a wandering MglB cluster stabilizes at one future cell pole and
194 positions MglA to the opposite future pole.

195 To investigate whether pole-like local cell curvature stabilizes MglB clusters, we
196 quantified the localization of stationary MglB clusters with regard to the geometry of
197 spores. We divide the spore/cell envelope into four quarters. In the quarter that
198 contained stationary MglB clusters, we defined the long and short axes as 0° and 90°,
199 which mark the local curvature that shows the highest and lowest similarity to the poles
200 of vegetative cells, respectively. As shown in Fig. 3E, MglB clusters stabilized randomly
201 in Phase I spores, indicating that MglB stabilizes before the establishment of cell poles
202 and that local curvature does not dictate the stabilized localization of MglB. The
203 population of diffusive MglB clusters decreased dramatically in the presence of A22,
204 mecillinam, cefmetazole and cefsulodin (Fig. 3D), indicating that in Phase I of
205 germination, active PG growth prevents MglB clusters from settling down. After the
206 stabilization of MglB, the sites harboring MglB clusters transformed into poles (0°) in
207 Phase II cells (Fig. 3E).

208 MglB clusters could stabilize either at the sites where PG synthesis has completed
209 or at the sites where PG synthesis has not yet initiated. We ruled out the second
210 possibility because the majority of MglB clusters (76.4%, n = 106) stabilizes at poles in
211 Phase II (Fig. 3A, 3B), where PG growth has completed (Fig. 1E). Consistent with our

212 finding that the Rod system becomes the dominant system for PG growth in Phase II
213 (Fig. 1H), A22 and mecillinam further reduced the small population of diffusive MglB
214 clusters in Phase II, while cefmetazole and cefsulodin did not show significant effects
215 (Fig. 3D). Taken together, it is the progress of PG growth, rather than the geometry of
216 the spore, that defines cell polarity. As MglB clusters only stabilize at the sites where
217 PG growth is completed, a region where PG synthesis completes first in Phase I will
218 become a future cell pole.

219 **The MglA-MglB polarity axis regulates PG synthesis by the Rod system through**
220 **MreB and the gliding motor.** MglA and MglB are both cytoplasmic proteins, which are
221 not likely to regulate the enzymatic activities of the Rod system directly. To investigate
222 whether MglA and MglB regulate the distribution of the Rod complexes, we used a fully
223 functional, photoactivatable mCherry (PAmCherry)-labeled MreB variant (17) to mark
224 the localization of Rod complexes in germination Phase II. When the majority of
225 PAmCherry was photoactivated, MreB-PAmCherry appeared as small patches (17)
226 (Fig. 4A). Compared to the wild-type spores where MreB patches mainly localized at
227 nonpolar locations, many MreB patches formed near cell poles and bulges of the
228 emerging *ΔmglA* and *ΔmglB* cells (Fig. 4A). We then photoactivate a few MreB-
229 PAmCherry particles in each emerging cell and quantified their localization using photo-
230 activatable localization microscopy (PALM). Along the long cell axis, we defined a
231 region within 320 nm from each end of cell as the pole and the rest of the cell as the
232 nonpolar region. In the emerging cells from wild-type spores that expressed MreB-
233 PAmCherry, the ratio between nonpolar and polar-localized MreB fractions was 2.68 (n
234 = 573, Fig. 4B). In contrast, in the *ΔmglA* and *ΔmglB* backgrounds, this ratio decreased

235 to 1.06 (n = 713) and 1.41 (n = 812), respectively (Fig. 4B). Our data support that during
236 the sphere-to-rod transition, MglA and expel MreB, and thus the Rod system, from cell
237 poles.

238 MglA connects MreB to the gliding motors and the gliding motors drive the
239 movement of MreB filaments (16, 17, 20). To test if MglA recruits the gliding motors to
240 transport the Rod complexes to nonpolar locations through MreB, we investigated the
241 regrowth process of the *ΔaglQS* pseudospores. *ΔaglQS* cells carry truncated gliding
242 motors that are unable to drive the rapid motion of MreB filaments (17). Due to the
243 truncation of motors, the *ΔaglQS* pseudospores lack compact polysaccharide layers on
244 their surfaces (32). Phenocopying the *ΔmglA* and *ΔmglB* spores, elongation of *ΔaglQS*
245 pseudospores delayed significantly and many emerging cells displayed bulged surfaces
246 in Phase II (Fig. 2). Consistently, significantly higher PG growth and MreB localization
247 were observed at cell poles and bulges in the elongation phase (equivalent to Phase II
248 of germination), similar to the observation made in *ΔmglA ΔdacB* and *ΔmglB ΔdacB*
249 spores (Fig. 2D, 4A, 4B). In summary, MglA and mglB restrict PG growth to nonpolar
250 regions in germination Phase II utilizing the gliding motors, which transport the Rod
251 complexes under the control of MglA.

252 **Discussion**

253 As spheres and rods are among the most common shapes adopted by walled bacteria,
254 the sphere-to-rod transition during *M. xanthus* spore germination provides a unique
255 opportunity to study rod-like morphogenesis in bacteria. Due to the absence of PG,
256 glycerol-induced *M. xanthus* spores are especially valuable for the study of *de novo* PG
257 synthesis, which drives spontaneous cell elongation in homogenous environments. In
258 contrast to fruiting bodies that require millions of cells and days to form, glycerol-
259 induced sporulation mimics the natural process that individual *M. xanthus* cells form
260 spores within hours in response to environmental stresses. Without the protection from
261 the fruiting body, rapid elongation could be critical for the survival of individual *M.*
262 *xanthus* spores.

263 Based on the mutually exclusive localization of MglB and MglA-GTP in vegetative
264 cells, we propose a model for spontaneous cell elongation during *M. xanthus* spore
265 germination (Fig. 4C). We observed that MglB forms wandering clusters in Phase I of
266 germination. Emerging cells start to elongate when the clusters of MglB stop moving
267 and stabilize at what is to become a future pole. An important clue for understanding
268 this process is that active PG growth prevents MglB clusters from settling down. Thus,
269 the wandering dynamics of MglB clusters serves as a mechanism to survey the status
270 of PG growth and the region where PG growth completes first in Phase I will host a
271 MglB cluster and become a future pole in Phase II. MreB plays a key role in the
272 stabilization of MglB clusters because both MglA and the Rod complexes assemble on
273 MreB. Since MglB avoids colocalizing with MglA-GTP by converting the latter to MglA-
274 GDP (18, 19) and MglA only binds to MreB (which also carries the Rod complexes) in

275 its GTP-bound form (16), the mutual exclusion between MglB and MglA-GTP will expel
276 MglB clusters from the Rod complexes. Once an MglB cluster stabilizes at one pole, the
277 expulsion between MglB and MglA-GTP causes MglA-GTP to cluster at the opposite
278 side of the spore (Figure 7). Then the diametrically opposing clusters of MglA-GTP and
279 MglB establish the polarity axis of the emerging cell.

280 A surprising finding of this work reveals that the MglA-MglB polarity axis regulates
281 the distribution of Rod complexes through the gliding machineries. Essential for gliding
282 motility, MreB serves as the platform for the assembly of the gliding machineries (12,
283 33). For this reason, compared to its homologs in other bacteria, *M. xanthus* MreB
284 displays unique dynamics: it is transported rapidly by the gliding motors, with a
285 maximum velocity of near 3 μm/s (17). At cell poles, MglA-GTP stimulates the assembly
286 of the gliding machinery by directly connecting it to MreB (12, 16). Once assembled, the
287 gliding machineries transport MreB filaments, thus entire Rod complexes, to nonpolar
288 locations (Figure 7) (17, 20). Utilizing the same system that defines the leading-lagging
289 axis in vegetative cells, spherical spores grow their walls at nonpolar regions and
290 eventually form rods.

291 Consistent with our model, the connection between the Rod complexes and gliding
292 machineries was also observed in a recent report, which showed that PG stops growing
293 in vegetative cells when the gliding machineries are dedicated to gliding (12). The
294 mechanism by which the gliding machineries switch between gliding and PG growth
295 remains to be investigated. Nonetheless, our results have added another layer to the
296 striking versatility of the gliding motors, which transport various cargos in different
297 compartments of the cells: spore coats on cell surfaces (32), the Rod complex and

298 gliding proteins in the membrane and periplasm (12, 15), as well as MreB and gliding

299 proteins in the cytoplasm (12, 17, 34).

300 **Materials and Methods**

301 **Strain construction.** Deletion and insertion mutants were constructed by
302 electroporating *M. xanthus* cells with 4 μg plasmid DNA. Transformed cells were plated
303 on CYE plates supplemented with 100 μg/ml sodium kanamycin sulfate or 10 μg/ml
304 tetracycline hydrochloride. In-frame deletion of *dacB* is described in *SI Appendix,*
305 *Materials and Methods, Table S2.*

306 **Sporulation, spore purification and germination.** Vegetative *M. xanthus* cells were
307 grown in liquid CYE medium (10 mM MOPS pH 7.6, 1% (w/v) Bacto™ casitone (BD
308 Biosciences), 0.5% yeast extract and 4 mM $MgSO_4$) at 32 °C, in 125-ml flasks with
309 rigorous shaking, or on CYE plates that contains 1.5% agar. When the cell culture
310 reaches OD_{600} 0.1 – 0.2, glycerol was added to 1 M to induce sporulation. After rigorous
311 shaking overnight at 32 °C, remaining vegetative cells were eliminated by sonication
312 and sonication-resistant spores were purified. Sonication-resistant spores were
313 collected by centrifugation (1 min, 15,000 g and 4 °C). The pellet was washed three
314 times with water. More details of spore purification and the purification of *ΔaglQS*
315 pseudospores are provided in *SI Appendix, Materials and Methods.*

316 **Microscopy Analysis.** Cryo-ET was performed on a Polara G2™ electron microscope.
317 Images were collected at 9,000× magnification and 8-μm defocus, resulting in 0.42
318 nm/pixel. Data were acquired automatically with the SerialEM software (35). Time-lapse
319 videos of the germination progress of wild-type and *ΔmglA* spores were recorded using
320 an OMAX™ A3590U CCD camera and a Plan Flour™ 40×/0.75 Ph2 DLL objective on a
321 phase-contrast Nikon Eclipse™ 600 microscope. The length, width and geometric
322 aspect ratios (L/W) of spores/cells were determined from differential interference

323 contrast (DIC) images using a custom algorithm written in MATLAB (The MathWorks,
324 Inc., Natick, MA), which is available upon request. DIC images of spores/cells were
325 captured using a Hamamatsu ImagEM X2™ EM-CCD camera C9100-23B (effective
326 pixel size 160 nm) on an inverted Nikon Eclipse-Ti™ microscope with a 100× 1.49 NA
327 TIRF objective, which are also used for capturing regular fluorescence and PALM
328 images. MglB clusters and single-molecules were localized using an algorithm written in
329 MATLAB (17), which is available upon request. More detailed information is provided in
330 *SI Appendix, Materials and Methods.*

References

1. A. J. Meeske *et al.*, SEDS proteins are a widespread family of bacterial cell wall polymerases. *Nature* **537**, 634-638 (2016).
2. P. D. A. Rohs *et al.*, A central role for PBP2 in the activation of peptidoglycan polymerization by the bacterial cell elongation machinery. *PLoS Genet* **14**, e1007726 (2018).
3. S. van Teeffelen, L. D. Renner, Recent advances in understanding how rod-like bacteria stably maintain their cell shapes. *F1000Res* **7**, 241 (2018).
4. B. P. Bratton, J. W. Shaevitz, Z. Gitai, R. M. Morgenstein, MreB polymers and curvature localization are enhanced by RodZ and predict *E. coli*'s cylindrical uniformity. *Nature communications* **9**, 2797 (2018).
5. A. Colavin, H. Shi, K. C. Huang, RodZ modulates geometric localization of the bacterial actin MreB to regulate cell shape. *Nature communications* **9**, 1280 (2018).
6. S. Hussain *et al.*, MreB filaments align along greatest principal membrane curvature to orient cell wall synthesis. *Elife* **7** (2018).
7. T. S. Ursell *et al.*, Rod-like bacterial shape is maintained by feedback between cell curvature and cytoskeletal localization. *Proc Natl Acad Sci U S A* **111**, E1025-1034 (2014).
8. F. Wong, E. C. Garner, A. Amir, Mechanics and dynamics of translocating MreB filaments on curved membranes. *Elife* **8** (2019).
9. R. M. Morgenstein *et al.*, RodZ links MreB to cell wall synthesis to mediate MreB rotation and robust morphogenesis. *Proc Natl Acad Sci U S A* 10.1073/pnas.1509610112 (2015).
10. H. Cho *et al.*, Bacterial cell wall biogenesis is mediated by SEDS and PBP polymerase families functioning semi-autonomously. *Nat Microbiol* 10.1038/nmicrobiol.2016.172, 16172 (2016).
11. T. K. Lee, K. Meng, H. Shi, K. C. Huang, Single-molecule imaging reveals modulation of cell wall synthesis dynamics in live bacterial cells. *Nature communications* **7**, 13170 (2016).
12. L. M. Faure *et al.*, The mechanism of force transmission at bacterial focal adhesion complexes. *Nature* **539**, 530-535 (2016).
13. E. M. Mauriello *et al.*, Bacterial motility complexes require the actin-like protein, MreB and the Ras homologue, MglA. *Embo J* **29**, 315-326 (2010).
14. B. Nan *et al.*, Flagella stator homologs function as motors for myxobacterial gliding motility by moving in helical trajectories. *Proc Natl Acad Sci U S A* **110**, E1508-1513 (2013).
15. B. Nan *et al.*, Myxobacteria gliding motility requires cytoskeleton rotation powered by proton motive force. *Proc Natl Acad Sci U S A* **108**, 2498-2503 (2011).
16. A. Treuner-Lange *et al.*, The small G-protein MglA connects to the MreB actin cytoskeleton at bacterial focal adhesions. *J Cell Biol* **210**, 243-256 (2015).
17. G. Fu *et al.*, MotAB-like machinery drives the movement of MreB filaments during bacterial gliding motility. *Proc Natl Acad Sci U S A* **115**, 2484-2489 (2018).
18. S. Leonardy *et al.*, Regulation of dynamic polarity switching in bacteria by a Ras-like G-protein and its cognate GAP. *Embo J* **29**, 2276-2289 (2010).

377 19. Y. Zhang, M. Franco, A. Ducret, T. Mignot, A bacterial Ras-like small GTP-
378 binding protein and its cognate GAP establish a dynamic spatial polarity axis to
379 control directed motility. *PLoS Biol* **8**, e1000430 (2010).
380 20. B. Nan *et al.*, The polarity of myxobacterial gliding is regulated by direct
381 interactions between the gliding motors and the Ras homolog MglA. *Proc Natl*
382 *Acad Sci U S A* **112**, E186-193 (2015).
383 21. D. R. Zusman, A. E. Scott, Z. Yang, J. R. Kirby, Chemosensory pathways,
384 motility and development in *Myxococcus xanthus*. *Nat Rev Microbiol* **5**, 862-872
385 (2007).
386 22. M. Dworkin, S. M. Gibson, A System for Studying Microbial Morphogenesis:
387 Rapid Formation of Microcysts in *Myxococcus xanthus*. *Science* **146**, 243-244
388 (1964).
389 23. E. I. Tocheva *et al.*, Peptidoglycan transformations during *Bacillus subtilis*
390 sporulation. *Mol Microbiol* **88**, 673-686 (2013).
391 24. K. Khanna *et al.*, The molecular architecture of engulfment during *Bacillus subtilis*
392 sporulation. *Elife* **8** (2019).
393 25. N. K. Bui *et al.*, The peptidoglycan sacculus of *Myxococcus xanthus* has unusual
394 structural features and is degraded during glycerol-induced myxospore
395 development. *J Bacteriol* **191**, 494-505 (2009).
396 26. Y. P. Hsu *et al.*, Full color palette of fluorescent d-amino acids for in situ labeling
397 of bacterial cell walls. *Chem Sci* **8**, 6313-6321 (2017).
398 27. E. Kuru *et al.*, In Situ probing of newly synthesized peptidoglycan in live bacteria
399 with fluorescent D-amino acids. *Angew Chem Int Ed Engl* **51**, 12519-12523
400 (2012).
401 28. M. F. Dion *et al.*, *Bacillus subtilis* cell diameter is determined by the opposing
402 actions of two distinct cell wall synthetic systems. *Nat Microbiol* 10.1038/s41564-
403 019-0439-0 (2019).
404 29. D. Keilberg, K. Wuichet, F. Drescher, L. Sogaard-Andersen, A response
405 regulator interfaces between the Frz chemosensory system and the MglA/MglB
406 GTPase/GAP module to regulate polarity in *Myxococcus xanthus*. *PLoS Genet* **8**,
407 e1002951 (2012).
408 30. C. B. Pogue, T. Zhou, B. Nan, PlpA, a PilZ-like protein, regulates directed motility
409 of the bacterium *Myxococcus xanthus*. *Mol Microbiol* **107**, 214-228 (2018).
410 31. Y. Zhang, M. Guzzo, A. Ducret, Y. Z. Li, T. Mignot, A dynamic response regulator
411 protein modulates G-protein-dependent polarity in the bacterium *Myxococcus*
412 *xanthus*. *PLoS Genet* **8**, e1002872 (2012).
413 32. M. Wartel *et al.*, A versatile class of cell surface directional motors gives rise to
414 gliding motility and sporulation in *Myxococcus xanthus*. *PLoS Biol* **11**, e1001728
415 (2013).
416 33. B. Nan, Bacterial Gliding Motility: Rolling Out a Consensus Model. *Curr Biol* **27**,
417 R154-R156 (2017).
418 34. M. Sun, M. Wartel, E. Cascales, J. W. Shaevitz, T. Mignot, Motor-driven
419 intracellular transport powers bacterial gliding motility. *Proc Natl Acad Sci U S A*
420 **108**, 7559-7564 (2011).

35. D. N. Mastronarde, Automated electron microscope tomography using robust prediction of specimen movements. *Journal of Structural Biology* **152**, 36-51 (2005).

ACKNOWLEDGEMENTS

We thank Drs. Joseph Sorg and Ritu Shrestha for their help in the initial determination of germination phenotypes, Drs. Michael Van Nieuwenhze and Yen-Pang Hsu for providing TADA, and Drs. David Zusman, Michael Manson and Joseph Sorg for critical reading of this manuscript. This work is supported by the National Institute of Health R01GM129000 (to B.N.) and R01AI087946 (to J.L.) and by CNRS to T.M.

431 **Figure Legends**

432 **Figure 1. PG polymerization by the Rod complex is essential for *de novo***
433 **establishment of rod-shape. A)** Morphological changes of untreated (UT) and
434 inhibitor-treated wild-type spores in the germination process. Mecillinam (MEC, 100
435 μg/ml), A22 (100 μg/ml) cefmetazole (CMZ, 5 mg/ml), cefsulodin (CSD, 5 mg/ml) and
436 fosfomycin (FOF, 8 mg/ml). **B)** Quantitative analysis of the germination progress using
437 the aspect ratios (L/W) of spores/cells. Boxes indicate the 25th - 75th percentiles,
438 whiskers the 5th - 95th percentiles. In each box, the midline indicates the median and ×
439 indicates the mean (Also see Table S1). Outlier data points are shown as individual dots
440 above and below the whiskers. **C)** Some oval spores initiate elongation along their short
441 axes during Phase II of germination (also see Movie S2). **D)** Phase I spores become
442 more spherical after 1-h treatments by mecillinam and A22 but initiate elongation earlier
443 when treated by cefmetazole. **E)** Patterns of PG growth in both phases of germination
444 were visualized by TADA labeling in *ΔdacB* spores. The average and standard deviation
445 of TADA intensity were calculated from 20 spores/cells in the diagrams to the right
446 (same below). **F)** Imaged at different focal planes, 22.0% of Phase I spores show bright
447 TADA patches (arrows) that position randomly on spore surfaces. **G)** Among these
448 22.0% spores, many contain multiple TADA patches. **H)** Compared to untreated (UT)
449 *ΔdacB* spores, while neither MEC, CMZ or CSD is able to block PG growth, the
450 combination of all three antibiotics (+3) abolishes PG growth in Phase I of germination.
451 In contrast, MEC alone is sufficient to inhibit PG growth in Phase II. Scale bars, 2 μm. *p*
452 values were calculated using the Student paired *t* test with a two- tailed distribution
453 (same below). NS, nonsignificant difference.

454 **Figure 2. MglA and MglB are required for rapid cell elongation. A)** Emerging cells
455 from *ΔmglA*, *ΔmglB, mglA*^{Q82L} spores and *ΔaglQS* pseudospores show significant delay
456 in elongation and crooked morphology in Phase II of germination. **B)** Quantitative
457 analysis of the germination progress. **C)** A representative image of the altered
458 morphology of the emerging *ΔmglA* cells after 3-h of germination. Arrows point to the
459 bulges that appear as additional poles. **D)** The disruption of either the MglA-MglB polar
460 axis (*ΔmglA ΔdacB* and *ΔmglB ΔdacB*) or the gliding motor (*ΔaglQS ΔdacB*) resulted in
461 significantly stronger PG growth at cell poles and budges (arrows) in Phase II.
462 Quantitative analysis of TADA fluorescence is shown on the right. Scale bars, 2 μm.
463 **Figure 3. MglB determines the first future pole. A, B)** While MglB-mCherry forms
464 clusters in Phase I spores (L/W ≤ 2), MglA-YFP are largely diffusive in Phase I. Without
465 MglB, MglA-YFP forms significantly less clusters in Phase II. For (**B**), the total number
466 of spores/cells analyzed for each strain is shown on top of the bar. **C)** 77.1% of MglB
467 clusters (red arrow) showed "wandering" dynamics in Phase I spores. In Phase II, MglB
468 clusters (yellow arrow) stabilized at cell poles and oscillated between opposite poles. As
469 a control, a TADA patch (white arrow) on a Phase I spore did not move during the entire
470 imaging process. **D)** The wandering behavior of MglB clusters depends on PG growth
471 as the inhibitors of PG synthesis, A22, MEC, CMZ and CSD, all significantly inhibit the
472 wandering of MglB in Phase I. In contrast, as the Rod system becomes the dominant
473 PG synthesis machinery in Phase II, only A22 and MEC inhibit the wandering of MglB in
474 Phase II. For each treatment, the total number of MglB clusters analyzed is shown on
475 top of the bar. UT, untreated. **E)** The stabilization of MglB clusters at cell poles does not
476 depend on local curvature. Scales bars, 2 μm.

477 **Figure 4. The MglA-MglB polarity axis regulates PG growth through MreB and the**
478 **gliding motor. A)** In the emerging *ΔmglA*, *ΔmglB* and *ΔaglQS* cells in Phase II of
479 germination, MreB patches (arrows) are frequently detected near cell poles and bulges.
480 **B)** The nonpolar-to-polar distribution ratios of MreB molecules were quantified by
481 PALM. For each strain, the total number of MreB particles analyzed is shown on top of
482 the bar. **C)** A schematic model for the *de novo* establishment of rod-shape by the MglA-
483 MglB polarity axis. Scales bars, 2 μm.

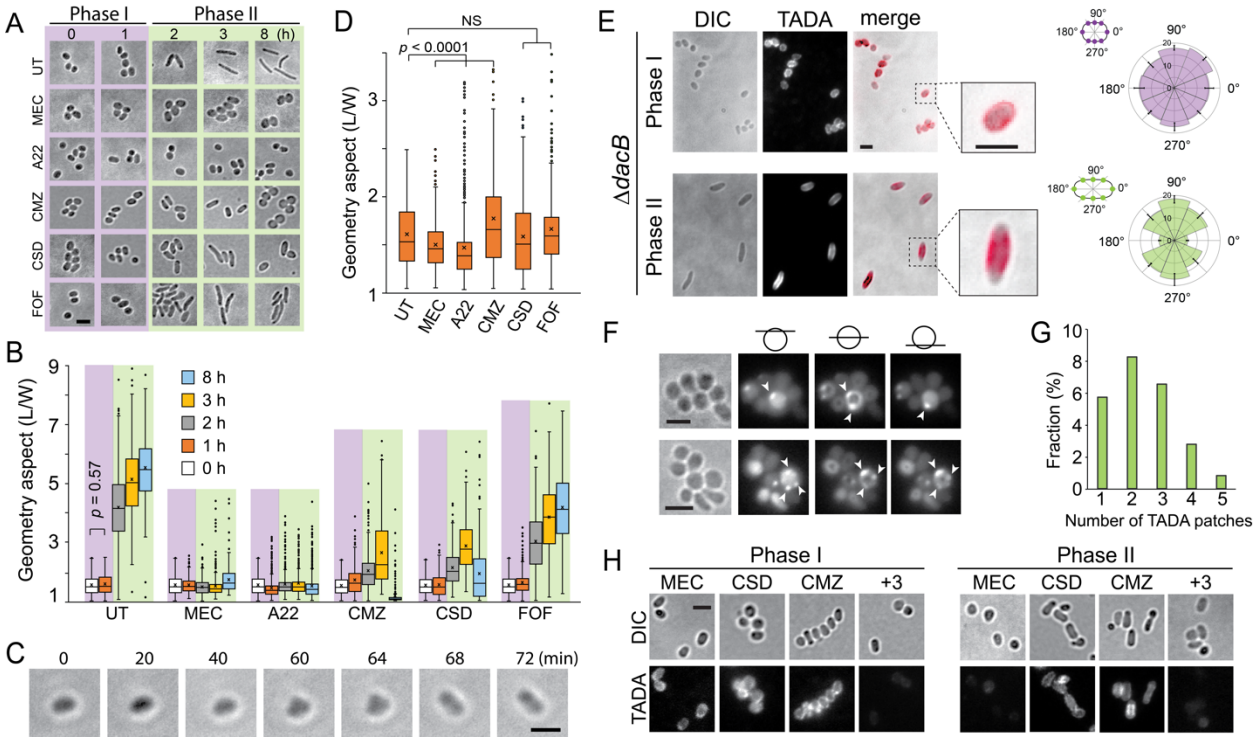
A
Phase I
Phase II
0
1
2
3
8 (h)
UT
MEC
A22
CMZ
CSD
FOF
D
NS
p < 0.0001
Geometry aspect (L/W)
UT
MEC
A22
CMZ
CSD
FOF
B
Geometry aspect (L/W)
8 h
3 h
2 h
1 h
0 h
p = 0.57
UT
MEC
A22
CMZ
CSD
FOF
C
0
20
40
60
64
68
72 (min)
E
DIC
TADA
merge
ΔdacB
Phase I
Phase II
90°
180°
0°
270°
F
G
Fraction (%)
Number of TADA patches
H
Phase I
Phase II
MEC
CSD
CMZ
+3
DIC
TADA

Fig. 1

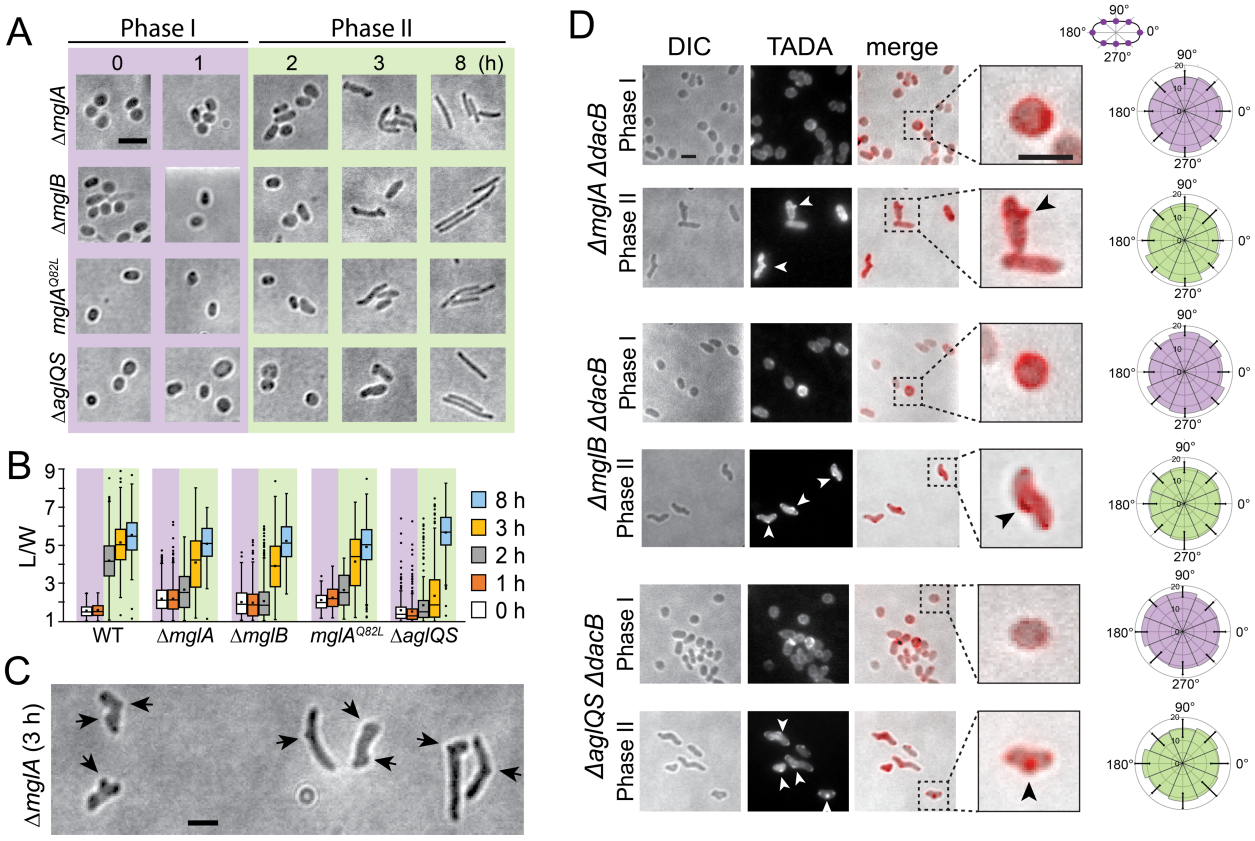
A
Phase I
Phase II
0
1
2
3
8 (h)
ΔmglA
ΔmglB
mglA^Q82L
ΔaglQS
B
L/W
9
7
5
3
1
8 h
3 h
2 h
1 h
0 h
WT
ΔmglA
ΔmglB
mglA^Q82L
ΔaglQS
C
ΔmglA (3 h)
D
DIC
TADA
merge
ΔmglA ΔdacB
Phase I
Phase II
ΔmglB ΔdacB
ΔaglQS ΔdacB
90°
180°
0°
270°

Fig. 2

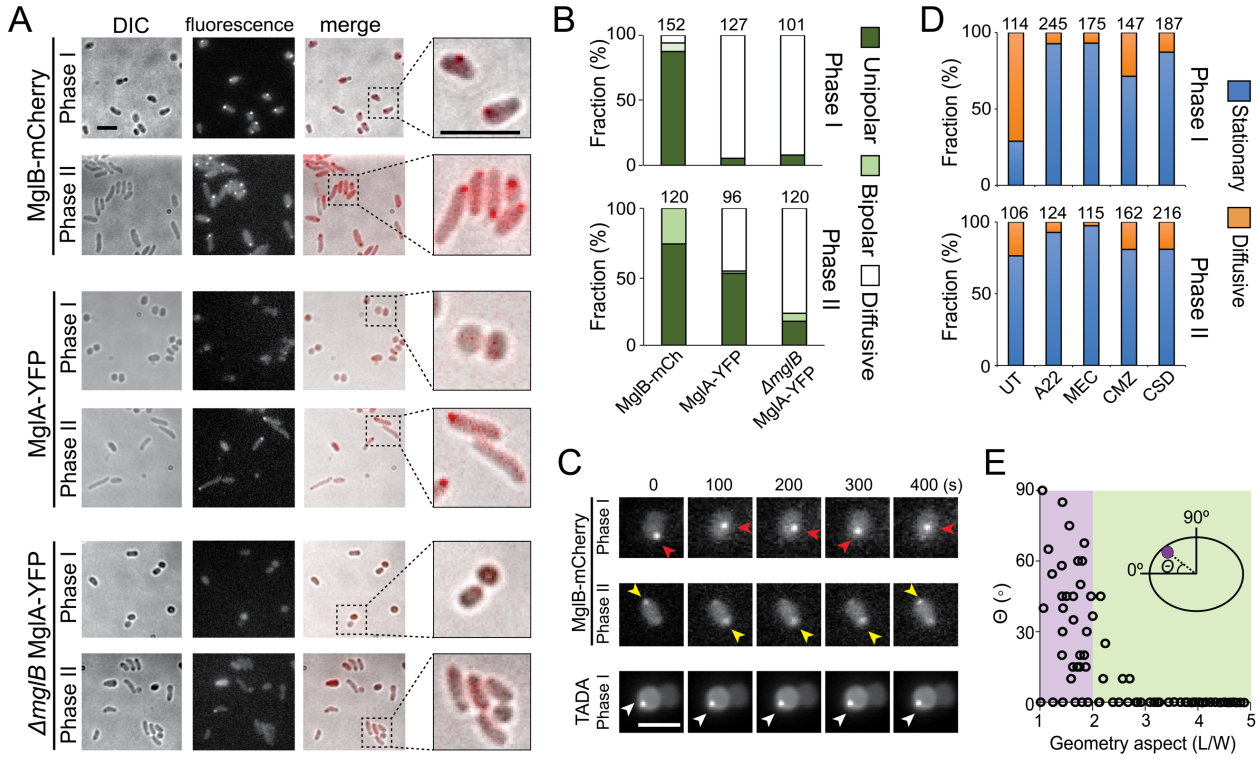
A
DIC
fluorescence
merge
MglB-mCherry
Phase I
Phase II
MglA-YFP
Phase I
Phase II
ΔmglB MglA-YFP
Phase I
Phase II
B
152
127
101
120
96
120
Fraction (%)
100
50
0
Phase I
Phase II
Unipolar
Bipolar
Diffusive
MglB-mCh
MglA-YFP
ΔmglB MglA-YFP
D
114
245
175
147
187
106
124
115
162
216
Stationary
Diffusive
UT
A22
MEC
CMZ
CSD
C
0
100
200
300
400 (s)
TADA
E
90
60
30
0
Θ (°)
90°
0°
Geometry aspect (L/W)
1
2
3
4
5

Fig. 3

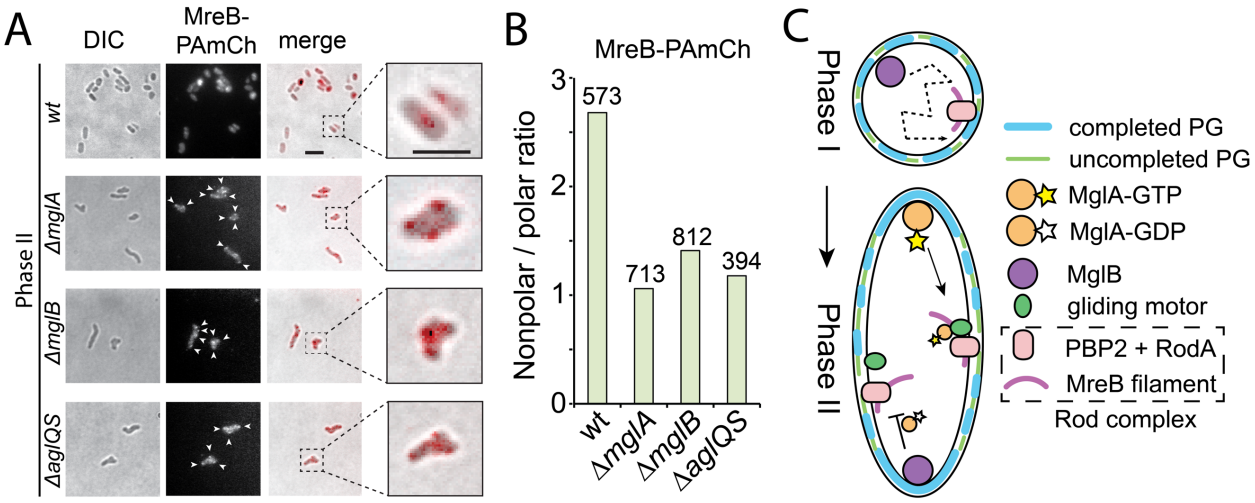
A
DIC
MreB-PAmCh
merge
Phase II
wt
ΔmglA
ΔmglB
ΔaglQS
B
MreB-PAmCh
Nonpolar / polar ratio
3
2
1
0
573
713
812
394
wt
ΔmglA
ΔmglB
ΔaglQS
C
Phase I
Phase II
completed PG
uncompleted PG
MglA-GTP
MglA-GDP
MglB
gliding motor
PBP2 + RodA
MreB filament
Rod complex

Fig. 4

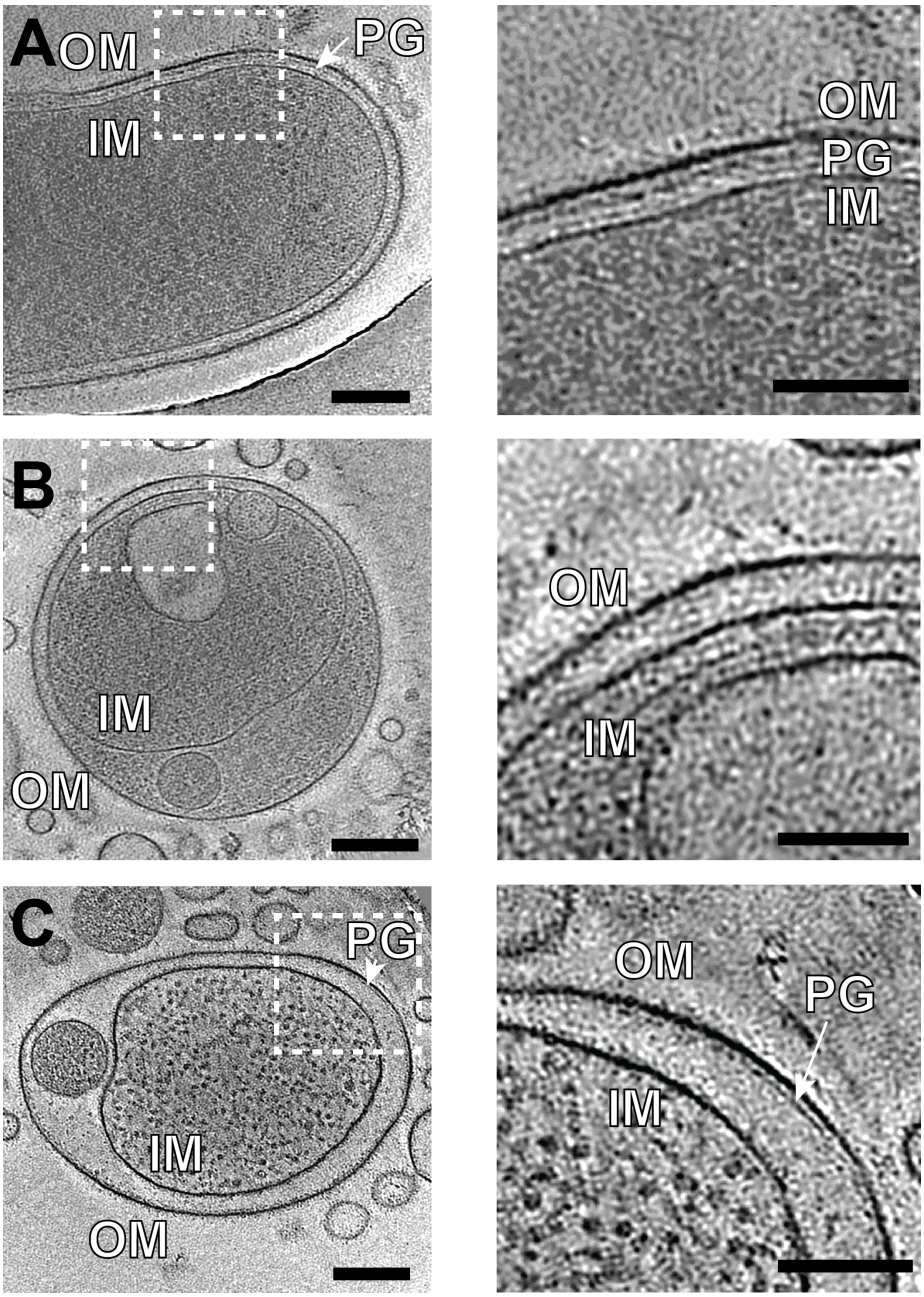

Fig. S1

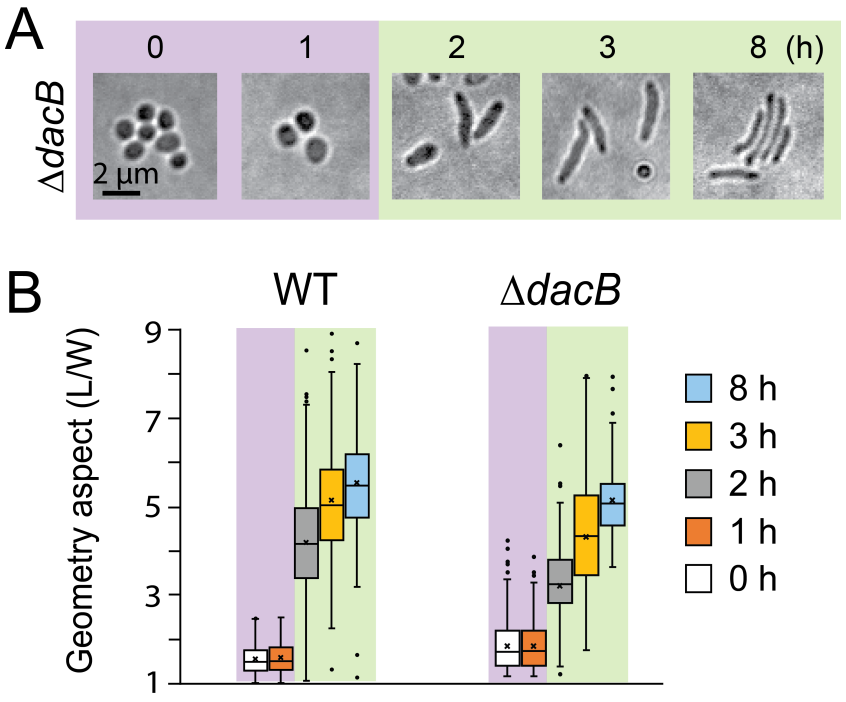
A
0
1
2
3
8 (h)
ΔdacB
2 µm
B
WT
ΔdacB
Geometry aspect (L/W)
9
7
5
3
1
8 h
3 h
2 h
1 h
0 h

Fig. S2

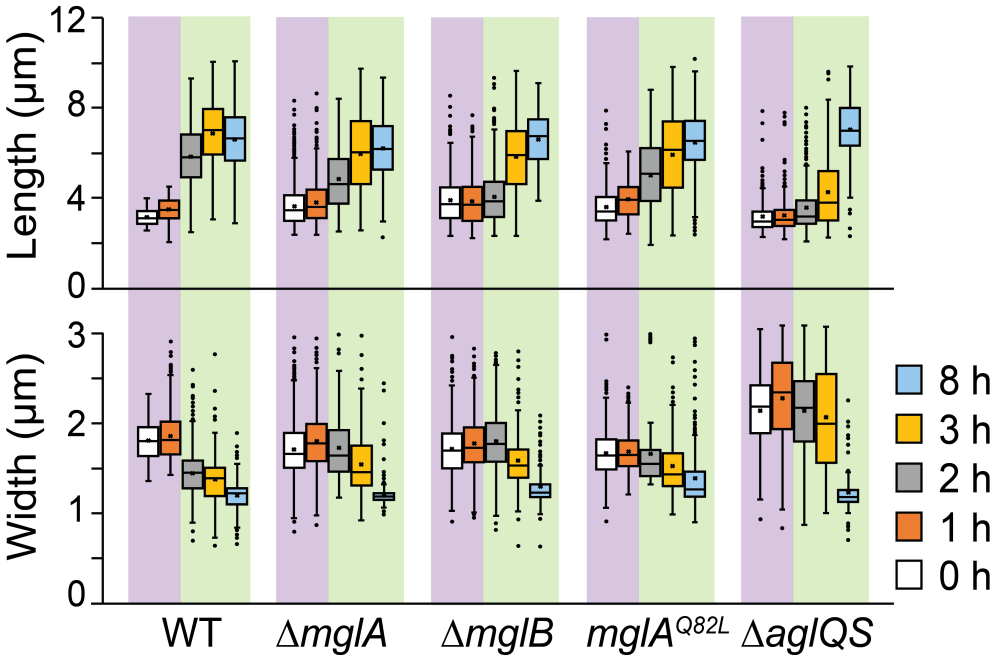
Length (μm)
12
8
4
0
Width (μm)
3
2
1
0
8 h
3 h
2 h
1 h
0 h
WT
ΔmglA
ΔmglB
mglA^Q82L
ΔaglQS

Fig. S3

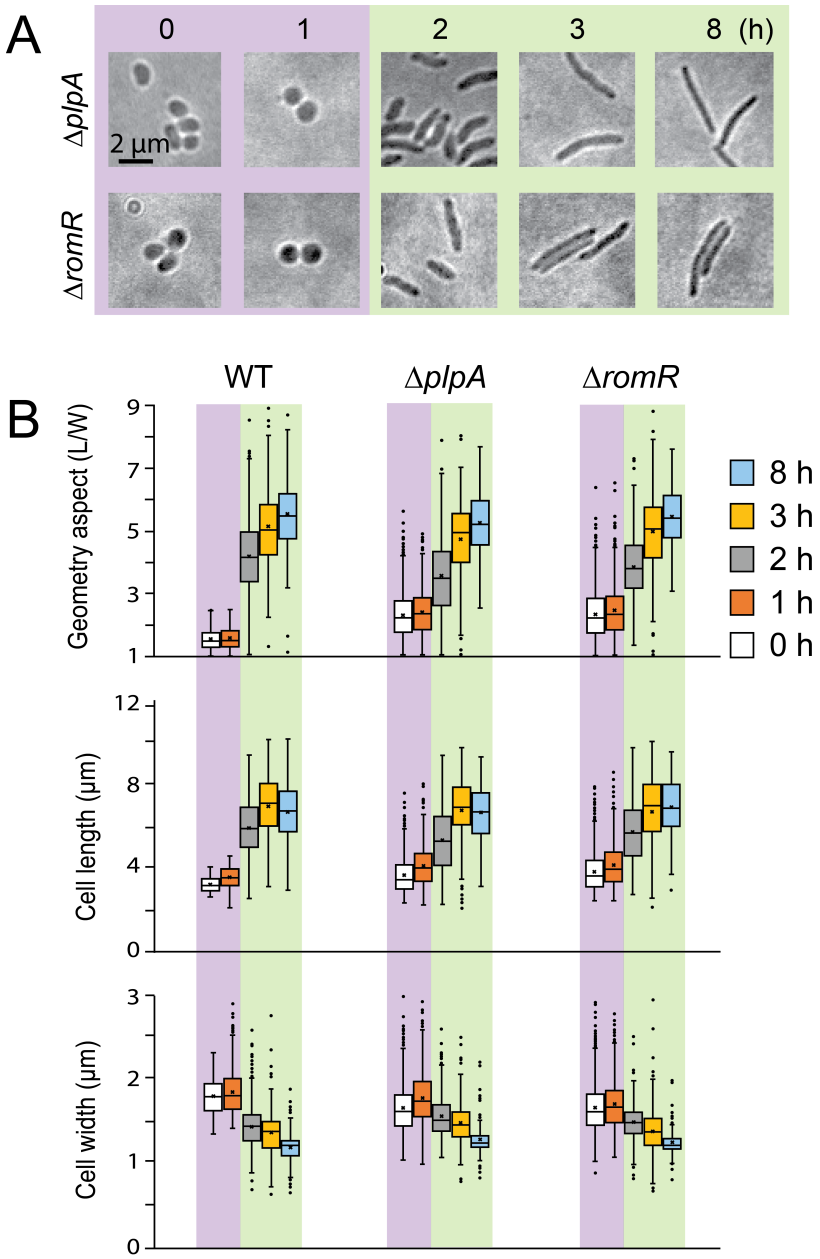
A
0
1
2
3
8 (h)
ΔplpA
ΔromR
2 μm
B
WT
ΔplpA
ΔromR
Geometry aspect (L/W)
Cell length (μm)
Cell width (μm)
8 h
3 h
2 h
1 h
0 h

Fig. S4